Thermodynamics and Kinetics of the Solid Solution of HCl in Ice

Emmanuel Thibert and Florent Dominé*,†

Laboratoire de Glaciologie et Géophysique de l'Environnement, CNRS, BP 96, 54 rue Molière, 38402 Saint Martin d'Hères Cedex, France

Received: July 15, 1996; In Final Form: February 18, 1997[⊗]

The equilibrium solubility of HCl in ice I_h has been measured as a function of temperature and HCl partial pressure, between −8 and −35 °C by doping large ice single crystals with gaseous HCl for several weeks. Results indicate that the solubility of HCl in ice is very low, much less than found in many previous studies. Its temperature and HCl partial pressure dependences are found to be $X_{HCl} = 6.13 \times 10^{-10} e^{2806.5/T} (P_{HCl})^{1/2.73}$ where X_{HCl} is the solubility in mole fraction, P_{HCl} is the HCl partial pressure in Pa, and T is the temperature in kelvin. The diffusion coefficient of HCl in ice is also found to be very low, about 10^{-12} cm^2/s at −15 °C. Extrapolations of these data yield the solidus in the temperature−composition phase diagram. The determination of the solid phase composition in equilibrium with a given gas phase composition allows the calculation of the partial enthalpy of sublimation of HCl from ice, $\Delta h^s_{HCl} = 63.7 \pm 7.6$ kJ/mol, and of the activity of HCl in ice. Possible mechanisms of HCl incorporation in ice are discussed. Atmospheric implications concerning ozone depletion and the understanding of snow composition are examined.

I. Introduction

I.a. Objectives. The chemical composition of ice is an important parameter involved in numerous processes of atmospheric sciences. Because of its physical and chemical properties and its common occurrence among atmospheric aerosols, ice plays a key role in atmospheric chemistry. Natural clouds (cirrus and convective clouds[1]) and anthropogenic tropospheric clouds (condensation trails of air planes[2]) at high altitude are made up of ice crystals. Ice clouds are also found at lower altitude in polar regions and in winter at middle latitudes. During their formation, ice crystals can trap atmospheric species that are initially present as trace gases and therefore modify atmospheric composition. This modification of the gas phase composition can also result from heterogeneous processes occurring on the surface of ice crystals.

It is indeed well established that such surface processes are involved in seasonal stratospheric polar ozone depletion.[3−5] The present understanding of this chemistry implies that forms of chlorine that are inactive in ozone destruction are activated on the surfaces of polar stratospheric clouds (PSCs), which are believed to be made up of particles consisting of liquid or solid mixtures of mostly H_2O and HNO_3 (refs 6−9, type I clouds), or water ice[10−12] (type II clouds).

Some of the heterogeneous reactions that have been proposed involve HCl adsorbed on PSC particles:[13]

$$HCl(s) + ClONO_2(g) \rightarrow Cl_2(g) + HNO_3(s) \qquad (R1)$$

In reaction R1, gaseous $ClONO_2$ reacts with HCl adsorbed on the surface of a PSC particle to produce an HNO_3 molecule incorporated in the aerosol and release a Cl_2 molecule to the gas phase, which is subsequently photolyzed into chlorine atoms that destroy ozone via gas phase catalytic cycles.[14]

The rate of reaction R1 depends on the uptake of HCl by ice and by H_2O-HNO_3 aerosols. At present, this parameter cannot be quantified by *in situ* measurements but is only accessible by laboratory experiments and thermodynamic calculations. These laboratory measurements must include surface and volume uptake measurements, as an accurate evaluation of the HCl surface concentration of PSC particles requires the knowledge of the partitioning of HCl between (i) the gas phase, (ii) the particle surface, and (iii) the particle volume.

Predicting the uptake of HCl by the volume of stratospheric ice particles obviously requires the measurement of the solubility of HCl in ice. However, because the formation of these HCl-doped ice particles in the stratosphere may involve nonequilibrium processes, the diffusion coefficient of HCl in ice must also be known to quantify HCl incorporation into stratospheric ice particles.[15]

Properties of $HCl-H_2O$ solid binary mixtures are also of interest to predict snow composition. The chemical composition of snow is indeed the result of numerous processes occurring in ice clouds, during precipitation and during snow aging after deposition. Moreover, the analyses of ice cores drilled in ice caps have the potential to yield detailed information on past atmospheric composition.[16] However, the relation linking atmospheric and ice compositions (called the air−snow transfer function) is complex for gaseous species such as HCl and HNO_3, and other polar molecules that interact strongly with ice.[17−19]

HCl is one of the main mineral acids that, together with HNO_3 and H_2SO_4, control the acidity of the atmosphere. The main natural source of HCl is sea salt aerosol fractionation: sea salt droplets emitted by the action of wind at ocean surfaces evaporate and form sea salt aerosol. Its Cl/Na ionic composition is close to that of bulk sea water[20] (1.8 weight ratio).

However, marine aerosols can show a depletion of chloride explained by the action of H_2SO_4 and HNO_3 which release HCl to the gas phase:[21,22]

$$2NaCl(aerosol) + H_2SO_4(aerosol) \rightarrow Na_2SO_4(aerosol) + 2HCl(gas) \qquad (R2)$$

$$NaCl(aerosol) + HNO_3(gas\ or\ aerosol) \rightarrow NaNO_3(aerosol) + HCl(gas) \qquad (R3)$$

Sea salt aerosol fractionation can occur with variable efficiency depending on climatic and transport conditions of sea salt aerosols. Analyses of ice cores drilled in East Antarctica have shown that during past very cold climatic periods or in

† E-mail: florent@glaciog.ujf-grenoble.fr.

⊗ Abstract published in *Advance ACS Abstracts,* April 1, 1997.

S1089-5647(96)02115-3 CCC: $14.00

winter snow layers, sea salt fractionation reactions were not very efficient and the Cl/Na weight ratio is close to 1.8 (ref 23). On the contrary, summer snow layers exhibit an excess of chloride (the ratio is higher than 1.8) present as HCl (ref 24). The Cl/Na ratio has been found to be lower than 1.8 in regions of central Antarctica with very low snow accumulation rate, where HCl initially incorporated in summer snow is supposed to have been released from the snow cover during the winter, when low partial pressures of HCl, P_{HCl}, prevail.[25]

Among the numerous processes involved during incorporation (predeposition processes) and during snow cover aging (post-deposition processes) such as adsorption, cocondensation, recrystallization or sublimation, an important parameter that can help understand snow composition is the thermodynamic equilibrium solubility of HCl in ice which is a function of P_{HCl} and temperature.

Knowing the solubility of HCl (and of other acids) in ice is also of interest to hydrological applications. The initial fractions of meltwater from natural snow are reported to have ionic concentrations higher than those of the snow they originate from.[26,27] This early release of chemical species such as SO_4^{2-} and NO_3^- and to a lesser extent Cl^- from the snowpack is called the ionic pulse. Since these anions are present as acids, this ionic pulse is often detected as an acidic pulse, which can result in lake acidification, with important ecological consequences. The reasons why acids are released early in snow melt are not clear,[28−31] but it has been suggested that this could be explained by considering the solubilities of acids in ice.[32]

I.b. Previous Studies. The first studies of the $HCl-H_2O$ binary system focused on the temperature−composition phase diagram and the determination of its crystallization points. In the mole fraction range 0−33% HCl, Pickering[33] determined the region of stability of 2 congruently melting solids: the HCl trihydrate ($HCl\cdot 3H_2O$) and the HCl dihydrate ($HCl\cdot 2H_2O$). Rupert[34] completed this diagram and found the region of existence of the HCl monohydrate ($HCl\cdot H_2O$). Vuillard[35] reported the existence of the HCl hexahydrate ($HCl\cdot 6H_2O$), which is difficult to nucleate. More recent studies[36] have confirmed those results concerning the liquidus composition and completed the phase diagram with investigations at lower temperatures and of metastable phases. The $HCl-H_2O$ phase diagram for low HCl composition is reported in Figure 1 with data from Vuillard[35] and Ji.[36]

By the early 1960s, ice was reported not to be able to dissolve any compounds[37] except NH_4F, NH_3, and HF (refs 38−40). These mixtures, called *solid solutions* by analogy with the liquid phase, had solute concentrations of the order of 10^{-4} mole fraction. During the 1960s and the 1970s, investigations on the incorporation of electrolytes in ice showed that ice was able to form solid solutions with species such as HCl, LiF, NaF, or KF which are weakly soluble in ice.[41]

HCl can dissolve in ice and form a solid solution up to a maximum concentration called the saturation solubility of HCl in ice. Above this limit, a new condensed phase of higher HCl concentration forms. This new phase can be an aqueous solution or the HCl hexahydrate, depending on the temperature. Because the saturation solubility is reached at a point where ice coexists with another phase, the phase rule implies that the system has only one degree of freedom. Variations of the saturation solubilities could be described by a function of, for example, temperature or the HCl partial pressure, P_{HCl}, since both these variables are linked on the coexistence curve. We have chosen to describe the variations of the saturation solubility as a function of temperature, and we will denote it as $S(T)$, as shown in Table 1 along with the other symbols used in this study. At

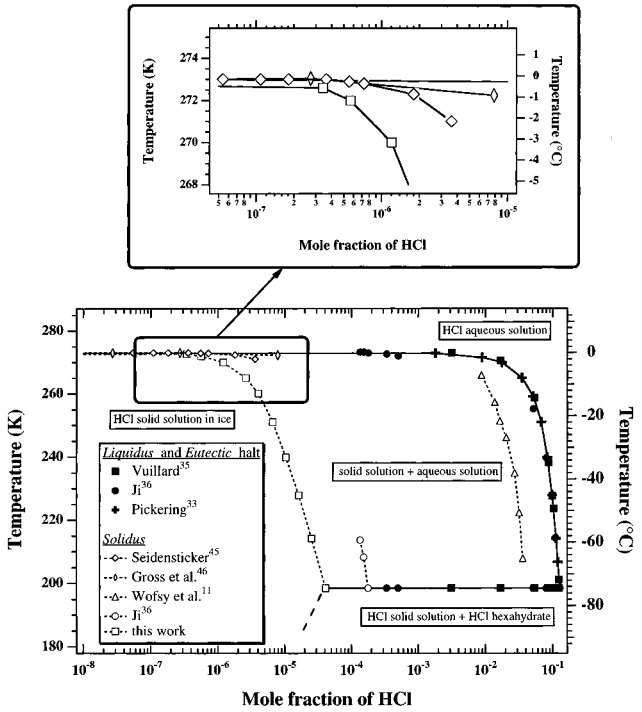

Figure 1. $HCl-H_2O$ temperature−composition phase diagram (logarithmic scale) at low HCl mole fraction. Dashed lines are the solidus lines. Open symbols: solidus curves; full symbols: liquidus curves and eutectic line.

TABLE 1: Symbols

symbol	definition
D	diffusion coefficient of HCl in ice
P_{HCl}	partial pressure of HCl
$P^*_{ice}(T)$	vapor pressure of pure ice
P'^*_{HCl}	vapor pressure of pure liquid HCl
T	temperature
$X_{HCl}(T,P_{HCl})$	mole fraction of HCl in ice
$S(T)$	saturation solubility of HCl in ice, i.e. X_{HCl} on the solidus line
K	solid to liquid partition coefficient of HCl
n	ice vapor pressure depression factor
Δh^s_{HCl}	partial molar enthalpy of sublimation of HCl from ice
Δh^v_{HCl}	partial molar enthalpy of vaporization of HCl from water
Δh^m_{HCl}	partial molar enthalpy of mixing of HCl in ice
a_{HCl}	activity of HCl in ice
γ_{HCl}	activity coefficient of HCl in ice

temperatures above the ice hexahydrate eutectic temperature (−74.7 °C), ice saturated with HCl coexists with a liquid solution, and $S(T)$ is given by the solidus line (Figure 1). Below the eutectic line, HCl-saturated ice coexists with the hexahydrate and $S(T)$ is given by the solvus line.[42]

In the solid solution domain of stability, the system has two degrees of freedom and the HCl content of ice is a function of two variables: temperature and P_{HCl}. The equilibrium composition is called solubility, written $X_{HCl} = X_{HCl}(T,P_{HCl})$ and expressed in mole fraction. It is clear that $X_{HCl}(T,P_{HCl}) \le S(T)$. Results available in the literature on HCl solid solutions in ice concern both the solidus composition and solubility.

Solidus Composition (Saturation Solubility). Krishnan and Salomon[43] measured the diffusion of HCl in ice single crystals by exposing them to an aqueous HCl solution, and calculated a solubility from their diffusion profiles. Their experimental setup allowed them to measure the solidus composition of ice, $S(T)$. They found a low value: 1.3×10^{-7} mole fraction, independent of temperature between −4 and −18 °C. De Micheli and Iribarne[44] studied the saturation solubilities of a few electrolytes

in ice samples consisting of very few crystals (i.e., almost single crystals) and their solid/liquid partition coefficient, defined at a given temperature as $K = S/X_{liq}$, where S and X_{liq} denote respectively the solid and liquid composition. K is a function of one variable (temperature or the composition of one of the two phases in equilibrium). The authors found for HCl a partition coefficient of 0.003 for an initial liquid concentration of 1.8×10^{-5} mole fraction. K was found to increase with increasing initial liquid concentrations. Seidensticker[45] also measured K for ice single crystals grown from aqueous HCl solutions and found that ice grown from concentrated solutions saturates at 3.6×10^{-6} mole fraction. Gross et al.[46] also measured K in ice single crystals or in "weakly polycrystalline" samples grown from HCl aqueous solutions. They obtained $K = 0.0027$, independent of concentration, and found a solubility limit of 8×10^{-6} mole fraction, obtained for [HCl] = 0.16 mol/L in the liquid. These three studies were over a temperature range of less than 1 K below the freezing point of pure water. Wolff et al.[47] studied the location and the diffusion of HCl in frozen aqueous solutions with a scanning electron microscope and an energy-dispersive X-ray microanalyzer. From measurements in the interior of a single crystal within their polycrystalline solid, they found $K < 0.002$ at −74.7 °C and a saturation solubility of less than 1.8×10^{-4} mole fraction. Wofsy et al.[11] measured the partition coefficient of HCl during the freezing of solutions between −6 and −66 °C and found $K = 0.3$ independent of concentration. Apparently, those authors were not aware of the much lower K values found earlier. A more recent study,[36] done on polycrystalline samples probably made up of very many small crystals, has focused on the solidus composition which has been directly investigated by thermal analysis (microcalorimetry and differential scanning calorimetry). The solidus composition was found to be 1.8×10^{-4} mole fraction of HCl at −60 °C ($K = 0.0017$). Most of these results are also shown in Figure 1.

Most of the above studies were done before the discovery of the ozone hole and by the late 1970s the interest in the study of the partitioning of electrolytes between water and ice had considerably decreased. With the discovery of the ozone hole, and the awareness that the interactions of acidic gases such as HCl with ice were key steps in ozone destruction chemistry, new studies started to take place in the late 1980s. For temperatures and HCl partial pressures typical of the polar stratosphere ($T \approx 190$ K and $P_{HCl} \approx 10^{-5}$ Pa), the equilibrium phase is indeed expected to be water ice including HCl in solid solution rather than HCl hydrates.[10,11,48] First studies of the solid solution, and not just of the solidus, were undertaken. In some studies, gaseous HCl, not aqueous solutions of HCl, were exposed to ice to determine its composition.

Solid Solution. Initial studies reported a large affinity for HCl with ice: Molina et al.[49a] exposed vapor-deposited polycrystalline ice to gaseous HCl, with partial pressure P_{HCl} between 1.3 and 133 Pa, and concluded that the solubility was very high (3×10^{-3} to 10^{-2} mole fraction at 200 K). They later realized[49b] that these high solubility values were erroneous and due to the formation of a metastable HCl liquid solution. They did not, however, propose a new solubility value in their later study. Wofsy et al.[11] measured the partition coefficient of HCl between ice and water and used their value ($K = 0.3$) and extrapolations of the data on HCl partial pressure over aqueous solutions obtained by Fritz and Fuget[50] to propose a $P_{HCl}-T$ diagram for the solid solution. From this, a solubility of about 0.02 mole fraction under stratospheric conditions was predicted. Later studies found lower solubilities for HCl in ice. In a preliminary study, Hanson and Mauersberger[48] exposed polycrystalline thin films to very low P_{HCl} and found a solubility of 2.9×10^{-4} mole fraction at 200 K under $P_{HCl} = 1.3 \times 10^{-5}$ Pa. In a subsequent paper, Hanson and Mauersberger[51] revised their initial results and reported a solubility of 9×10^{-5} mole fraction at 190 K and 2×10^{-5} Pa.

As indicated previously and reported in Figure 1, results available on the solidus composition and partition coefficient are widely scattered, which suggests the presence of experimental artifacts in at least some of these studies. The main reason that could explain those discrepancies is that initial studies have first investigated or used results from liquid−solid equilibria to predict gas−solid equilibria. Although thermodynamics allows such calculations, measurements of liquid−solid partition coefficients are often difficult because of the presence of artifacts at the liquid−solid interface.[52] These artifacts, which include an unstable growth interface resulting in the occlusion of concentrated liquid solutions, may be responsible for some of the scatter. Attempts to derive gas−solid partition coefficients from liquid−solid and gas−liquid equilibria may then be affected by those artifacts.

In order to avoid those difficulties, we have designed a new method which directly investigates gas−solid equilibria. Preliminary results[15,18] have shown that the solubility of HCl in ice was low in the adopted experimental conditions and remained low if extrapolated to atmospheric conditions. Because most of our early results were obtained at −15 °C, it was not possible to obtain thermodynamic parameters of the HCl−ice binary mixture. New data have now been obtained over a wider $T-P_{HCl}$ range, and the partial enthalpies of sublimation and of mixing of HCl in ice have been calculated. Atmospheric implications of these results regarding ozone depletion, snow composition, and ice clouds composition are presented.

II. Experimental Section

The experimental method used to measure HCl solubility and diffusion in ice have been described only briefly in a preliminary paper,[15] and more details are therefore given here. Experiments are performed by doping laboratory-grown single crystals of ice with gaseous HCl. After doping, crystals are sliced and analyzed to determine the HCl diffusion profile which yields the solubility and the diffusion coefficient.

Ice Crystal Growth. Ice I_h crystallizes in the hexagonal structure with an hexagonal symmetry axis refered as the $\vec{c}$-axis (or optical axis). Ice crystals grown from liquid water usually have their $\vec{c}$-axis perpendicular to the growth direction[52] (i.e., usually horizontal). Initial growth without any seed crystal (using the modified Bridgman apparatus shown in Figure 2) produced such crystals from which seed crystals where carved and placed at the bottom of the plexiglass cylinder with their $\vec{c}$-axis vertical.

We used double-deionized water produced by a Millipore filtration system. The electric resistivity of the water was always more than 18 MΩ·cm. In order to avoid the inclusion of air bubbles in the crystal, water was degassed by boiling. The crystal seed of about 4 cm height was frozen at the bottom of a plexiglass tube 8 cm in diameter and 30 cm long, in a cold room at −15 °C. After thermal equilibrium in another cold room at 0 °C, the upper part of the tube was filled with water. In order to complete degassing, the tube was evacuated down to a residual pressure of 6 mbar. Then, the tube was set onto the Bridgman growth stage. The bottom of the tube was placed in the upper part of the cold bath, maintained at −18 °C, so that the top centimeter of the ice crystal seed melted and the water/ice boundary reached its equilibrium shape (Figure 2), which is controlled by heating with a resistor that also adjusts

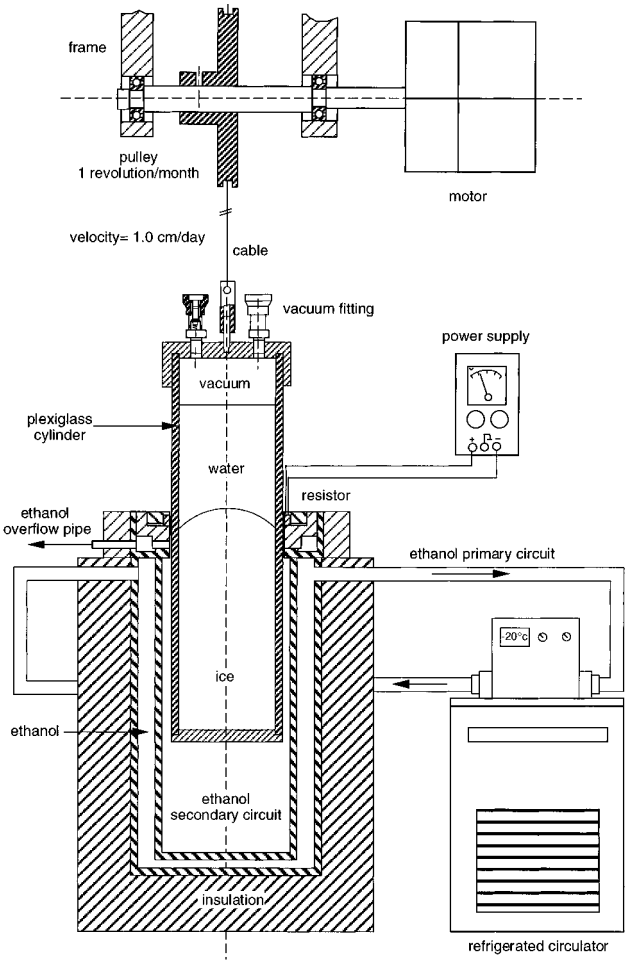

Figure 2. Experimental setup used for ice single crystal growth.

the temperature gradient at the ice−water boundary. The plexiglass tube was lowered in the cold bath at about 0.12 μm/s (1 cm/day). After 25 days, the water had completely crystallized and formed a single crystal of the required orientation. The tube was removed from the Bridgman growth stage and placed in the cold room at 0 °C. After thermal equilibrium was reached, a thin film of water formed between the ice sample and the plexiglass and the crystal could easily be removed from the tube.

Crystals were observed between crossed polaroids to control their single crystallinity and the $\vec{c}$-axis orientation. Some crystals showed small angle boundaries with such high disorientations that they were visible between polaroids. These crystals were discarded. Because of its very low yield stress (<0.01 MPa, ref 52), ice is very sensitive to dislocation multiplication processes and surface effects. In order to preserve their initial structure, selected samples were packed in polyethylene sealed bags and stored in one block at −25 °C.

In order to investigate the possible chemical contamination of ice during growth and storage, ionic impurity concentrations of selected samples were measured by ion chromatography. Only bulk concentrations were measured after surface decontamination by melting and rinsing with ultrapure water. The results are reported in Table 2. Beside chloride, species investigated were Na^+, NH_4^+, K^+, Mg^+, Ca^+, NO_2^-, NO_3^-, SO_4^{2-}, F^-, $HCOO^-$, CH_3COO^-, and CH_2OHCOO^-. $[H^+]$ was not measured but calculated from the ionic budget.

As shown in Table 2, the ice develops a low level of contamination during growth, while the reported species are not detectable in the water from which the ice is grown. This contamination probably occurs when water is in contact with the plexiglass tube (as reported by Legrand et al.[53] for carboxylic acids). However, this contamination can be safely neglected when compared to the chloride concentrations that are expected.

TABLE 2: Concentration of Various Ions in Ice Single Crystals Used for Diffusion Experiments

cations	concn (mole frac × 10^{-10})	anions	concn (mole frac × 10^{-10})
Na^+	22.5	Cl^-	5.1
NH_4^+	20	F^-	6.6
K^+	10.7	$HCOO^-$	37.2
Mg^{2+}	7.4	CH_3COO^-	86.0
Ca^{2+}	9.2	CH_2OHCOO^-	8.1
		NO_2^-	2.2
		NO_3^-	3.6
$pH = 6.3^a$		SO_4^{2-}	8.1

[a] $[H^+]$ was not measured but calculated from the ionic budget.

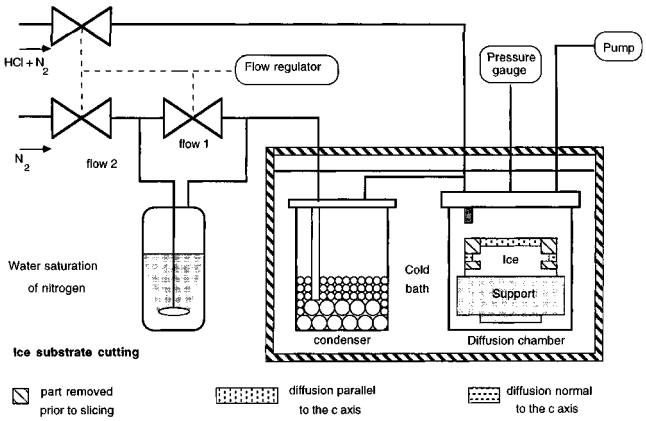

Figure 3. Experimental set up to study HCl diffusion in ice. The lathing procedure after diffusion is also indicated.

Sample Machining. Before doping, crystals were cut in a cold room to a length of 4 cm. A lathe was used to give the crystals a perfect cylindrical shape and a flat surface. In order to have a reproducible position of the sample on the lathe before and after doping, the mandrel was replaced by a stainless steel support on which the ice sample was frozen (Figure 3). The support was screwed directly on the shaft of the lathe. This setup gives a sample position reproducible within 5 μm along the axis and less than a $^1/_4$ of minute of angle between the sample and the lathe axis. This reproductibility is necessary for the determination of the diffusion profile and its mathematical treatment which yields the diffusion coefficient and the solubility. In order to minimize microcrack formation during lathing, samples were machined at low rotation velocity (around 150 rounds/min) and the tool's depth of penetration never exceeded 100 μm.

Doping. After machining, samples were placed in a stainless steel diffusion chamber immersed in a controlled temperature ethanol bath (Figure 3). To minimize the damage which may have been caused to the surface by machining (dislocations, microcracks), the crystals were annealed at −3 °C for about 15 h before doping. Because the velocity of dislocations in unstressed ice at that temperature is greater than 1 μm/s and that of small angle boundaries greater than 0.05 μm/s (ref 54), this duration should be sufficient to remove most of the dislocations generated by lathing in the first millimeter near the surface. The samples were then allowed to equilibrate at the temperature of the experiment for 2 h and exposed to a flow of HCl diluted in nitrogen. HCl partial pressure was obtained by using mixtures of 9 and 45 ppm (±5%) of HCl in N_2 from Alphagaz which were further diluted in nitrogen before reaching the diffusion chamber. The manufacturer's dilution values were

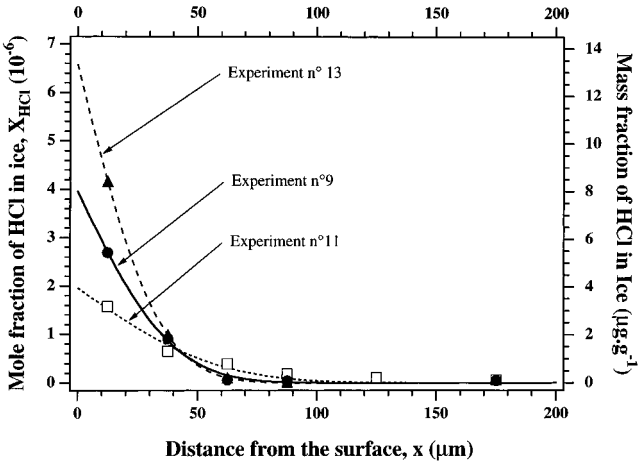

Figure 4. Typical experimental diffusion profiles of gaseous HCl in ice single crystals. Concentrations are corrected from the blank. Experimental conditions (temperature, HCl partial pressure, diffusion time) are detailed in Table 3. Lines are the fit of the data to eq 1.

checked by flowing those mixtures through water in a bubbler. The water was analyzed by ion chromatography and its chloride content was as predicted by the gas−liquid equilibrium values of Fritz and Fuget[50] within the 5% accuracy given by Alphagaz. The gas line was conditioned before the experiment under the same partial pressure conditions. In order to prevent the sublimation of the sample, part of the nitrogen flow (flow 2, see Figure 3) was diverted through a bubbler where it was saturated with water at 20 °C. The ratio flow 1/flow 2 was adjusted so that the nitrogen water content was slightly above the saturation vapor pressure of ice at the temperature of the experiment. The excess water was condensed in a stainless steel condenser packed with stainless steel balls before reaching the diffusion chamber. Because the condenser and the diffusion chamber were located in the same bath, it was found that this method was very accurate to control P_{H_2O}, except when excess ice accidentally blocked a condenser tubing, in which case the ice crystal could completely sublimate. Besides those accidents, we never observed any sublimation or condensation on the ice crystals that would have suggested imperfections in P_{H_2O} regulation. Variations of the height of the ice crystals could be checked within 5 μm from its positioning on the lathe.

Cutting Procedure. After a diffusion time of several weeks, the ice samples and their support were placed on the lathe again. In order to obtain two diffusion profiles (parallel and normal to the $\vec{c}$-axis), the region where HCl had diffused from both directions was removed as shown in Figure 3. The first profile (parallel to the $\vec{c}$-axis) was obtained by removing ice layers parallel to the flat surface of the cylinder. These layers were retrieved as shavings in a container placed under the crystal. The profile normal to the $\vec{c}$-axis was obtained by removing concentric layers as indicated in Figure 3. The removed layers were 25−50 μm thick and the shavings retrieved from each layer weighted 50−90 mg. Shavings were melted and diluted in 2 mL of deionized water. Solutions were analyzed in a clean laboratory by ion chromatography (Dionex 2010i) where HCl was detected as chloride, using an AS4A anion separator column and a carbonate/dicarbonate eluent. This analysis gave the chloride content in each layer (typically 0.1−10 nmol). The mean concentrations of the layers were calculated from the weight of the shavings. Typical profiles of diffusion are shown in Figure 4. Because of the low HCl concentrations, we have performed blank measurements to avoid a systematic error due to a possible chloride contamination in the adopted analysis procedure.

The blank determinations were performed by removing layers from undoped single crystals on the lathe. The chloride contents in layers (typically 6×10^{-11} mol for 25 μm thick layers) were subtracted from the chloride content of experimental diffusion profiles. Blank values were generaly low (same order as the analytical detection limit) compared to diffusion profiles. Experimental profiles corrected from the blanks were fitted to eq 1:

$$X(x,t) = X_0\left[1 - \mathrm{erf}\left(\frac{x}{2\sqrt{Dt}}\right)\right] \qquad (1)$$

which is the solution to Fick's laws of diffusion for a semi-infinite solid exposed to a constant P_{HCl} (ref 55). In eq 1, $X(x,t)$ is the mole fraction of chloride at a distance x from the diffusion interface after a diffusion time t. X_0 is the concentration at $x = 0$. With the hypothesis that no surface processes are limiting the incorporation of HCl in the bulk ice, equilibrium is immediately reached near the surface. Therefore, X_0 is the equilibrium solubility which is a function of temperature and HCl partial pressure (constant for each experiment) and we therefore have $X_0 = X_{HCl} = X_{HCl}(T,P_{HCl})$. D is the diffusion coefficient of HCl in ice which depends on temperature, and erf is the error function.

As detailed in Dominé et al.,[15] diffusion profiles showed a systematic deviation from eq 1: for $x > 200$ μm, the concentration decrease was slower than predicted by eq 1. This is typical of diffusion along one- or two-dimensional defects that act as diffusion short circuits.[55] Small angle boundaries (planes formed by regrouped dislocations) are probably responsible for most of the fast diffusion at long distances. Thus, eq 1 was only used where it applied, i.e., in the first four to five points of the profiles, to obtain the solubility and the diffusion coefficient. This part of the profile is indeed little affected by diffusion short circuits.[56] Since the publication of our preliminary results,[15,18] we reduced the density of small angle boundaries in ice crystals by increasing the temperature of the cold bath used in the crystal growing apparatus from −23 to −18 °C. Moreover, the crystals were annealed at −3 °C for about 15 h before doping. Besides decreasing the density of small angle boundaries, this density probably became more reproducible with this treatment.

Error Analysis. The error of the analytical procedure takes account of errors in the chromatograph calibration ($2 \times \sigma_{calib} = 11.1 \times 10^{-11}$ mol for a 2 mL injection volume) and in variations in the chloride signal in the blanks ($2 \times \sigma_{blank} = 12 \times 10^{-11}$ mol). Other analytical errors are negligible, so that the overall error is $e = 2\sigma = 2[\sigma^2_{calib} + \sigma^2_{blank}]^{1/2} = 16.3 \times 10^{-11}$ mol which gives a concentration error of 5×10^{-8} mole fraction in ice in the first slices, and a detection limit of 1.8×10^{-8} mole fraction.

The temperature was regulated within 0.2 °C. Because the temperature dependence of our results is not large, the error due to temperature variations is small. P_{HCl} was accurate within 5%. The other important error is on the position of the cutting tool (5 μm). A sensitivity analysis was performed to evaluate the effects of these two sources of error on the determination of the solubility and diffusion coefficient by eq 1. The test was performed on a diffusion profile of low solubility (2×10^{-6} mole fraction) having a typical diffusion coefficient (10^{-12} cm^2/s). The resulting errors (2σ) are 15% for the solubility and 50% for the diffusion coefficient. Rather than a fit to eq 1, Krishnan and Salomon[43] used an integration method to determine D and X_{HCl}. Their method was tested and gave results similar to our fits.[15]

From these various sources of error we estimate that our error (2σ) are ±20% for the solubility and ±60% for the diffusion coefficient.

III. Results

As listed in Table 3, 14 diffusion experiments were performed under various conditions of temperature (from −8 to −35 °C) and HCl partial pressure, P_{HCl} (from 0.267×10^{-3} to 4×10^{-3} Pa). Diffusion was often measured both normal and parallel to the $\vec{c}$-axis which gave two independent measurements of the solubility for each experiment. Both measurements differ from each other by 7.5% on average, which supports the reliability of our solubility results.

Kinetics of Diffusion. The diffusion coefficients we have measured are very low. They are reported in Figure 5a as a function of temperature. Some experiments (symbol *a*, Table 3) were performed on crystals that were not annealed after machining. Despite the fact that we used only the first four or five points of each profile to determine *D*, the value obtained is slightly affected by the presence of diffusion short circuits.[15] The values of *D* that we obtained must therefore be considered as upper limits, and the true value of *D* in the −8 to −35 °C range is probably around 10^{-12} cm^2/s. Because the density of short circuits varies and is especially high for the unannealed samples, the *D* values we obtained are very scatterred, and as is obvious in Figure 5a, it is not possible to test whether the variations of *D* with *T* follow an Arrhenius law. It is interesting to note that the diffusion of HCl is greatly accelerated by the presence of short circuits. As we will report in future publications, the diffusion of other molecules is much less affected by short circuits.

Thermodynamics. HCl partial pressures occurring in the atmosphere (typically 10^{-5}−10^{-6} Pa) are lower than those used in our experiments. In order to predict the solubility at lower *T* and P_{HCl}, we have used thermodynamic relations to construct a pressure−temperature phase diagram. According to Gibbs's phase rule, a solid solution in equilibrium with the gas phase is a bivariant system which therefore has two degrees of freedom. Among the four variables that determine this system, *T*, X_{HCl}, P_{H_2O} and P_{HCl}, it is therefore possible to derive two relationships linking these variables. This derivation has already been done by Hanson and Mauersberger,[48] who used the Gibbs−Duhem relationship. They obtained

$$P_{HCl} = A(T)(X_{HCl})^n \quad (2)$$

$$P_{H_2O} = (1 - nX_{HCl})P^*_{ice}(T) \quad (3)$$

where $A(T)$ is a temperature-dependent coefficient, *n* is the ice vapor pressure depression factor and $P^*_{ice}(T)$ is the vapor pressure of pure ice. The parameter *n* also represents the number of structural entities created by the incorporation of HCl in ice.[45] These entities can be undissociated HCl, or the ions H^+ and Cl^- or structural defects such as Bjerrum L defects.[57] The determination of *n* from our data using eq 2 can therefore provide information on the mechanism of incorporation of HCl in ice.

The temperature dependence of $A(T)$ can be related to the partial molar enthalpy of sublimation of HCl, Δh^s_{HCl}, so that relation 2 can be written (using Clapeyron's law and the hypothesis that *n* and Δh^s_{HCl} are not temperature dependent):

$$P_{HCl}(X_{HCl},T) = A_0 e^{(-\Delta h^s_{HCl}/RT)}(X_{HCl})^n \quad (4)$$

where A_0 is a constant. Whether our data follow eq 4 has been

TABLE 3: Experimental Results of the Diffusion of Gaseous HCl in Ice between −8 and −35 °C

experiment no.	1[a]	2[a]	3	4	5	6[a]	7[a]	8[a]	9[a]	10	11	12	13	14	15	16	17	18	19	20	21[a]	22[a]
temperature (°C)	−8	−8	−8	−8	−7.5	−15	−15	−15	−15	−15	−15	−15	−25	−25	−25	−25	−35	−35	−35	−35	−35	−35
direction relative to the $\vec{c}$-axis	*b*	*c*	*b*	*c*	*b*	*c*	*b*	*c*	poly	*b*	*c*	*c*	*c*	*b*	*c*	*b*	poly	poly	poly	poly	*c*	*b*
P_{HCl} (10^{-3} Pa)	1.67	1.67	1.07	1.07	0.267	6.67	6.67	1.69	0.56	1.08	4	0.267	4	4	0.267	0.267	4	4	0.267	0.267	0.4	0.4
diffusion time (10^6 s)[d]	1.26	1.26	0.605	0.605	0.432	1.29	1.29	0.756	1.04	1.55	1.84	0.718	2.77	2.77	3.63	3.63	1.746	1.746	1.53	1.53	1.63	1.63
solubility $X_{HCl} \times 10^6$ (mole fraction)[e]	2.66	2.55	2.42	2.44	1.24	5.32	5.52	3.64	1.98	2.75	3.89	1.67	6.64	7.03	2.16	2.67	11.7	12.36	2.9	3.2	5.03	5.33
diffusion coefficient (10^{-12} cm^2/s)	2.8[a]	2.6[a]	6.4	7.2	7.8	14.5[a]	7.5[a]	13[a]	9.4[a]	2.3	2.8	5.0	1.2	1.1	8	6.8	4	4.4	5.0	6.2	10.7[a]	8.3[a]

[a] No annealing after machining and prior to doping. poly, polycrystals with grain size about 1 cm^2 were used in these experiments. [b] The direction of diffusion is normal to the $\vec{c}$-axis. [c] The direction of diffusion is parallel to the $\vec{c}$-axis. [d] 10^6 s ≈ 11.6 days. [e] HCl mole fraction: $10^{-6} \approx 5\ 10^{-5}$ mol/L of ice at 0 °C.

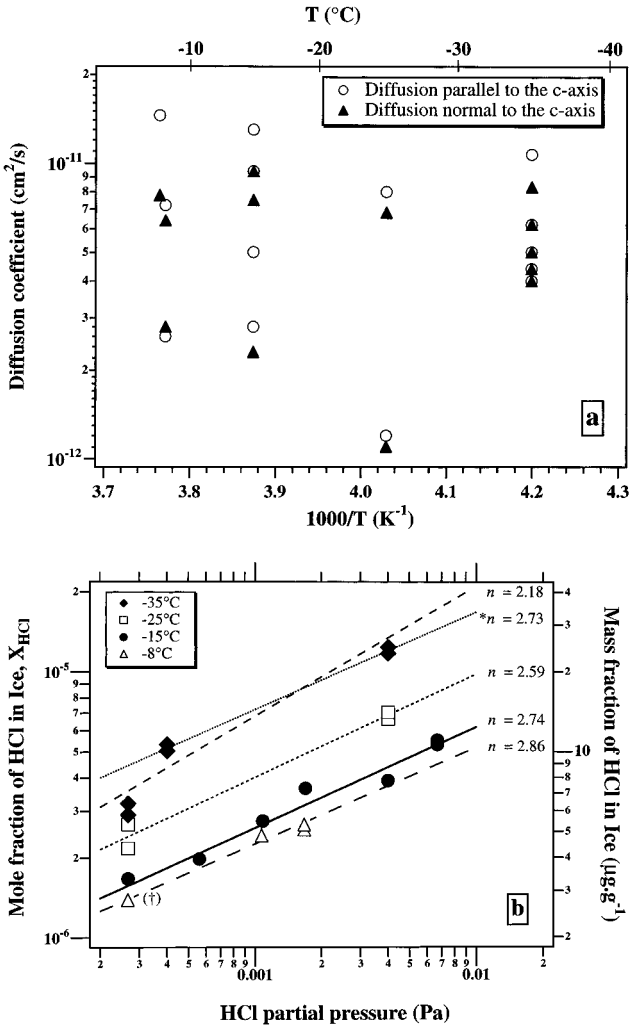

Figure 5. (a) Diffusion coefficient of HCl in ice vs temperature. The scatter is due to variable densities of diffusion short circuits in the various ice samples used (see text). (b) Equilibrium solubility of HCl (expressed in mole fraction and in mass fraction) in ice as a function of the partial pressure of HCl, P_{HCl}. For each temperature, the data have been fitted to eq 3. (†) The solubility value of experiment no. 5 performed at −7.5 °C, has been corrected using $\Delta h^s_{HCl} = 63.7$ kJ/mol, to determine n at −8 °C. (*) Fit of the data obtained at −35 °C excluding profiles 19 and 20.

tested and we have used two methods to determine A_0, Δh^s_{HCl}, and n from our results.

1. Determination of n and A(T) from Two Separate Linear Regressions. The parameter n can in fact be considered to be constant, i.e., independent of both composition and temperature. First, a composition dependence of n seems unlikely: because of the very low HCl concentration in ice, HCl is as if it was at infinite dilution and the types of interactions should not be concentration dependent in this range. This hypothesis is confirmed for aqueous solutions of HCl: n is constant ($n = 2$) in the composition range 0.0002−0.02 according to Fritz and Fuget's measurements.[50] At higher compositions n increases steeply. This composition dependence appears because Raoult's law is no longer obeyed. The water−hydrochloric acid binary system indeed displays a maximum boiling point at 14.8 wt % HCl (ref 58) which is typical of liquid phases that show negative deviation from ideality. Second, the fact that n is not composition dependent is supported by our results as shown in Figure 5 where the solubility has been plotted as a function of P_{HCl}. For each set of temperature, log X_{HCl} is a linear function (whose slope is $1/n$) of log P_{HCl}.

The parameter n can also be considered as independent of temperature. A temperature dependence of n will be related to a change in the mechanism of HCl incorporation in ice. This seems unlikely in the narrow temperature range considered. If anything, a temperature dependence might be possible very near the melting point, but we are interested here in extrapolating to low temperature. The data shown in Figure 5 and in Table 4 nevertheless indicate that n decreases weakly and monotonously with temperature from 2.86 ± 0.05 at −8 °C to 2.18 ± 0.25 at −35 °C. However, if analytical errors are taken into account, the signifance of this trend is mainly based on the value of n at −35 °C, which is itself very dependent on the value of the diffusion experiment performed at the lowest P_{HCl} (no. 19 and 20). It is difficult to explain why this experiment yielded low solubility values. This experiment was the first one to be performed with the mixture of 9 ppm of HCl in nitrogen, and it is possible that inadequate purging and conditioning of the gas line resulted in a P_{HCl} lower than expected, but this is only speculation. In any case, this experiment appears less reliable than the others, and we have chosen to eliminate it from our fits. A fit of the four other solubility values obtained at −35 °C gives $n = 2.73 \pm 0.02$. If profiles 19 and 20 are omitted, n is then independant of temperature in the experimental range. We will now refer to the values obtained without profiles 19 and 20 with the symbol *.

We also expect Δh^s_{HCl} to be independent of composition and temperature because HCl is practically at infinite dilution in ice, and because of the narrow temperature range. This was observed by Fritz and Fuget[50] for aqueous HCl solutions in the temperature range 0−60 °C, and also by Walrafen et al.[59] who measured HCl partial molar heat of evaporation (Δh^v_{HCl}) for concentrated solutions between 20 and 110 °C. Using mean values for n (2.59 and *2.73), Δh^s_{HCl} has been calculated on a HCl isobaric line according to the following relation obtained by taking the derivative of relation 4 with respect to $1/T$:

$$\left(\frac{\mathrm{d}\ln X_{HCl}}{\mathrm{d}(1/T)}\right)_{P_{HCl}} = +\frac{\Delta h^s_{HCl}}{nR} \qquad (5)$$

Solubilities calculated from the fit of our data (Table 4) at $P_{HCl} = 4 \times 10^{-3}$ Pa are plotted versus $1/T$ in Figure 6. The slope of the curve yields $\Delta h^s_{HCl}/nR$ (relation 5). Δh^s_{HCl} is found to be 61.8 ± 10.4 kJ/mol. Excluding profiles no. 19 and 20, we have $^*\Delta h^s_{HCl} = 63.7 \pm 7.6$ kJ/mol. Errors have been calculated from the linear regression (variables ln X_{HCl} and $1/T$) and defined as 2σ. The calculation of A_0 has been made with solubilities of HCl in ice under 4×10^{-3} Pa from relation 4. Results are reported in Table 5.

2. Three-Variables Least-Squares Method. A three-variables least-squares method has also been used to determine simultaneously the three parameters A_0, Δh^s_{HCl}, and n in eq 4. Calculations have also been made excluding experiments no. 19 and 20 as in the first method. Results are reported in Table 5. We have not calculated the errors on the parameters determined with this method. However, the values obtained here without profiles 19 and 20 are very similar to the values obtained with the first method. Moreover, the validity of the regression was checked with the χ^2 test. In both methods, the parameters are in good agreement since they yield a calculated solubility within the experimental error of the data (20%). Since the first method provides uncertainties on the three parameters and since we prefer to exclude profiles no. 19 and 20 because we feel that they are not as reliable as the other data, the pressure

TABLE 4: Fit of the Data to Eq 2 for Each Set of Temperature[c]

temp (°C)	−8[a]	−15	−25	−35	−35*
no. of diffusion profiles	5[a]	7	4	6	4*
$A(T)$ (Pa)	1.38×10^{13}	1.82×10^{12}	9.43×10^{10}	1.97×10^{8}	1.11×10^{11}
$n \pm 2\sigma$[b]	2.86 ± 0.05	2.74 ± 0.03	2.59 ± 0.03	2.18 ± 0.25	2.73 ± 0.02

[a] One diffusion profile was obtained at −7.5 °C and was corrected to obtain a solubility value at −8 °C (see text). [b] σ values do not include analytical errors. [c] Calculations marked * have been made without profiles 19 and 20.

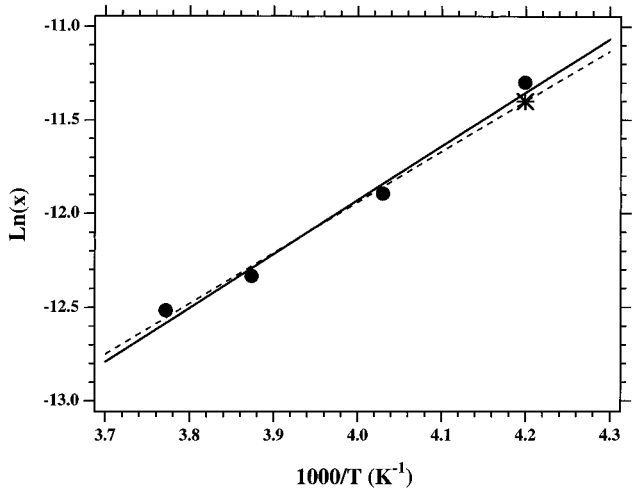

Figure 6. Solubilities of HCl in ice under $P_{HCl} = 4 \times 10^{-3}$ Pa versus inverse temperature. The slope of the line is equal to $\Delta h^s_{HCl}/vP$. The solid line is the fit of all the data. (*) Solubility at −35 °C and $P_{HCl} = 4 \times 10^{-3}$ Pa excluding profiles 19 and 20. The dashed line is the fit of the data excluding profiles 19 and 20.

TABLE 5: Determination of the Three Parameters A_0, Δh^s_{HCl}, and n according to the Two Methods[a]

	A_0 (Pa)	Δh^s_{HCl} (kJ/mol)	n
separate linear	$(8.56 \pm 0.94) \times 10^{23}$	61.8 ± 10.4	2.59 ± 0.26
regressions	$(1.41 \pm 0.31) \times 10^{25}$ *	63.7 ± 7.6*	2.73 ± 0.10*
three-variable	8.61×10^{21}	53.0	2.55
method	2.78×10^{24} *	62.2*	2.67*

[a] Calculations marked * are made without experiment no. 19 and 20.

and temperature dependence of the HCl mole fraction in ice that we will use later and which we recommend from our data is, with T in K and P_{HCl} in Pa:

$$X_{HCl} = 6.13\ 10^{-10}\ e^{(2806.5/T)}(P_{HCl})^{1/2.73} \quad (6)$$

Solubilities resulting from eq 6 are shown in Figure 7. This figure gives the variation of HCl partial pressure versus $1/T$ above aqueous solutions and solid solutions of given solubilities. As a consequence of relation 4, isosolubility curves are straight lines with slopes equal to $-\Delta h^v_{HCl}/R$ for aqueous solutions and $-\Delta h^s_{HCl}/R$ for solid solutions. Ice−water boundary has been calculated from extrapolations of Fritz and Fuget's data[50] and from the composition phase diagram reported in Figure 1. The Ice hexahydrate boundary is that determined by Wooldridge et al.[60]

Mixing Properties of the System. The partial molar enthalpy of mixing of HCl, Δh^m_{HCl}, and the enthalpy of formation of HCl at infinite dilution in ice $\Delta H^\infty_{HCl,ice}$ defined by the enthalpy of the reaction

$$^1/_2H_2 + {}^1/_2Cl_2 \rightarrow [HCl]^\infty_{ice} \quad (R4)$$

can be easily related to the partial molar enthalpy of sublimation

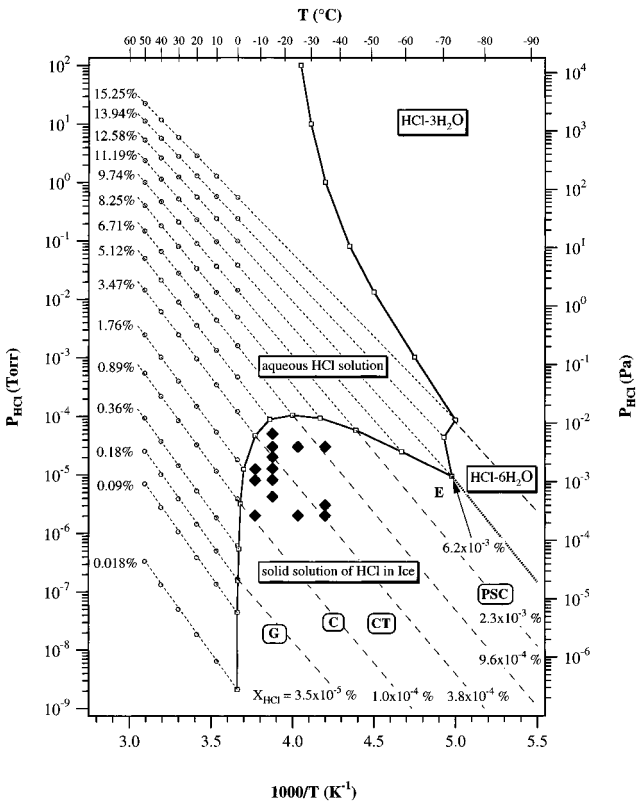

Figure 7. Isosolubility curves in mole fraction for HCl in ice and in aqueous solutions, as a function of P_{HCl} and inverse temperature: (◆) our experimental conditions, (○): Fritz and Fuget's experimental results for aqueous solutions. The solid line is the ice-water boundary from Pickering[33] and Vuillard.[35] The dotted line is the ice hexahydrate boundary from Wooldridge et al.[60] The letters G, C, CT, and PSC represent typical HCl partial pressure and temperature conditions encountered respectively in the Greenland troposphere, cirrus, condensation trail of airplanes, and type II polar stratospheric clouds.

that we have measured. The activity a_{HCl} of the solute in the solid solution is usually defined as

$$a_{HCl} = P_{HCl}/P'^*_{HCl} = \gamma_{HCl}X_{HCl} \quad (7)$$

where P'^*_{HCl} is the equilibrium vapor pressure of pure liquid HCl at the temperature of interest, γ_{HCl} is the activity coefficient. With this definition, γ_{HCl} assumes a value of 1 when HCl is pure (Raoultian standard state). The relation between chemical potential and activity coefficient is $\Delta\mu_{HCl} = \mu_{HCl} - \mu^0_{HCl} = RT \ln a_{HCl} = RT \ln \gamma_{HCl}X_{HCl}$, where μ^0_{HCl} refers to the chemical potential of HCl in its standard state. The variation of the activity coefficient with temperature can be calculated from the Gibbs−Helmholtz relation which applied to a given composition leads to

$$\left(\frac{\partial \ln a_{HCl}}{\partial T}\right)_{X_{HCl}} = \left(\frac{\partial \ln \gamma_{HCl}}{\partial T}\right)_{X_{HCl}} = \frac{H^0_{HCl} - h^m_{HCl}}{RT^2} = -\frac{\Delta h^m_{HCl}}{RT^2} \quad (8)$$

where H^0_{HCl} and h^m_{HCl} are the enthalpies of pure liquid HCl and

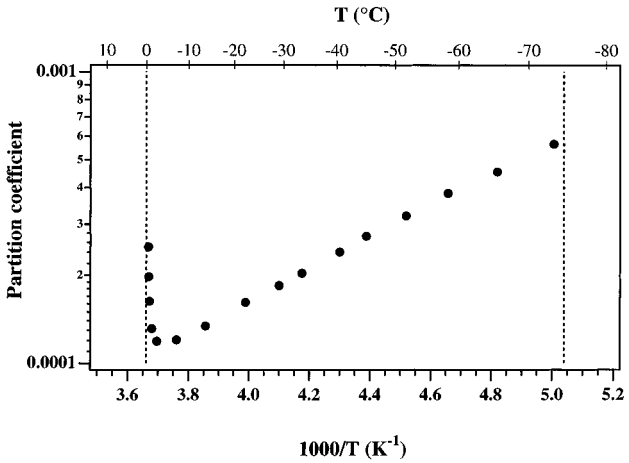

Figure 8. Calculated partition coefficient K vs temperature. Dotted lines are ice−water and ice−hexahydrate boundaries.

HCl in solid solution in ice. Δh^{m}_{HCl} is the partial molar enthalpy of mixing (standard state is pure liquid HCl). According to the definition of the activity of HCl, taking the derivative of relation 7 gives

$$\left(\frac{\partial \ln a_{HCl}}{\partial T}\right)_{X_{HCl}} = \left(\frac{\partial \ln P_{HCl}}{\partial T}\right)_{X_{HCl}} - \left(\frac{\partial \ln P'^{*}_{HCl}}{\partial T}\right)_{X_{HCl}} \quad (9)$$

From relations 8 and 9 the enthalpy of mixing of HCl in ice is $\Delta h^{m}_{HCl} = L^{v}_{HCl} - \Delta h^{s}_{HCl}$, where L^{v}_{HCl} is the heat of vaporization of pure liquid HCl (16.16 kJ/mol at −85 °C, ref 58). The partial molar enthalpy of mixing is therefore

$$\Delta h^{m}_{HCl} = -47.5 \pm 7.6 \text{ kJ/mol}$$

(standard state pure liquid HCl)

The enthalpy of formation of HCl in ice can be calculated from the transformation $HCl_{ice} \rightarrow HCl_{gas}$ (whose enthalpy is $\Delta h^{s}_{HCl} = 63.7 \pm 7.6$ kJ/mol) and from the enthalpy of formation of gaseous HCl which is -92.2 ± 1 kJ/mol (average value between −8 and −35 °C, calculated from ref 58). The enthalpy of the reaction of formation of HCl in ice at infinite dilution (R4) is therefore $\Delta H^{\infty}_{HCl,ice} = -155.9 \pm 8.6$ kJ/mol in the temperature range −8 to −35 °C.

Solidus Composition (Saturation Solubilities). The solidus composition calculated from the data of Figure 7 has been reported in Figure 1. The solidus composition predicted by our data together with the liquidus data of Vuillard[35] and Ji[36] have also been used to determine the partition coefficient. The temperature dependence of K is reported in Figure 8. Since we have studied solid−gas equilibrium, our partition coefficient has in fact been determined by an indirect method.

IV. Discussion

Diffusion Coefficient. Our values of the diffusion coefficient are much lower than those of Krishnan and Salomon,[43] who obtained $D = 2 \times 10^{-8}$ cm^2/s. As explained in Dominé et al.,[15] this value, associated with their very low solubility (1.2×10^{-7} mole fraction at the solidus between −4 and −18 °C) is more consistent with a surface diffusion process. These authors obtained their diffusion profiles by having HCl diffuse from a concentrated HCl solution frozen on their ice single crystal. We tried a similar method in preliminary studies and placed our samples in a cold room at −15 °C. Our interpretation of our observations was that the small variations (<0.5 °C) due to the temperature regulation result in a continuous melting and refreezing of the interface between the ice and the HCl reservoir (which is in fact polycrystalline ice with a concentrated liquid HCl solution at the grain boundaries[32]). Because these processes do not take place at equilibrium, inclusions of concentrated HCl solutions are trapped in the ice (constitutional supercooling, Hobbs[52]), which results in very high and irreproducible apparent solubility in the first layers analyzed. Only layers far enough from the surface have HCl values that can be treated as a diffusion profile. Krishnan and Salomon[43] only show data far from the interface, suggesting a problem with their data close to the interface, which they eliminated.

On the contrary, our values of D are higher than those of Wolff et al.[47] ($D < 10^{-13}$ cm^2/s at −20 °C). Considering the solubility that we have measured which is lower than their detection limit (1.8×10^{-4} mole fraction), they had no way to detect diffusion and their upper limit therefore has no basis. From HCl uptake on 0.3−0.5 μm thick ice films, Koehler et al.[61] have estimated that D is approximately 10^{-12} cm^2/s at 158 K. From our data, we would expect a lower value for D at this temperature. Their value is probably an overestimate because their ice samples were microcrystalline and the numerous grain boundaries doubtless acted as diffusion short circuits.[55] Our data of Table 3 show that small angle boundaries can result in an apparent value of D at least an order of magnitude larger than the true value, and grain boundaries are expected to have an even greater effect.

Our data (Figure 5a) do not show any anisotropy of diffusion of HCl in ice, but again our accuracy on D is not sufficient to reach a definite conclusion on this point.

Solidus Composition (Saturation Solubilities) and Partition Coefficient. Various authors[11,44−46] have attempted to measure the ice−water partition coefficient of HCl, K, by growing doped ice crystals from HCl liquid solutions. Because of the rejection of chloride by ice, a concentrated layer appears at the ice−water interface, and a concentration gradient of chloride develops in the liquid and generates diffusion. The measured partition coefficient is therefore the one which occurs between ice and this concentrated liquid layer.

The solute distribution in the liquid is determined by liquid phase diffusion, natural convection, and stirring when such a process is applied to reduce the concentration gradient near the interface. The two extremes of perfect mixing in the liquid[62] and of the solute transport by diffusion[63] have been theoretically investigated. Studies[11,44−46] have tried to perform experiments under conditions close to both these cases where partition coefficients can be calculated.

In Seidensticker's experiments,[45] the chloride which is rejected in the liquid layer is supposed to be transported by diffusion. K is determined from the liquid concentration calculated at the interface according to Tiller et al.'s theory[63] applied to that case. However, Tiller et al.'s expression assumes that K is not concentration dependent which is not supported by Seidensticker's results: K decreases from 2×10^{-2} to 1.8×10^{-4} with increasing liquid concentrations from 3×10^{-6} to 2×10^{-2} mole fraction. The calculated liquid concentration and the partition coefficient are therefore questionable. The highest solubility measured by Seidensticker was 3×10^{-6} mole fraction corresponding to a mole fraction in the liquid of 0.02. Beyond this value, ice growth probably became unstable and crystals then got milky. As observed in alloys solidification,[42] constitutional supercooling can occur which causes dendritic growth and interdendritic occlusion of liquid. The incorporation of the solute does not occur at equilibrium. This process probably acted as a practical limitation in Seidensticker's experiments.

In order to minimize the effects of the ice/water interface on the partitioning of chloride, Gross et al.[46] and DeMicheli and Iribarne[44] have performed experiments with very low freezing rates and stirring of the liquid solutions near the phase boundary. Their results are in reasonable agreement with Seidensticker[45] ($K = 3 \times 10^{-3}$ and a solubility limit of about 2×10^{-6} mole fraction) but they did not find any concentration dependence for K. However, even in such experiments, mixing of the liquid cannot be perfect and the existence of a thin concentrated liquid layer at the interface is probable. The measured partition coefficient will then be the effective coefficient[52] and K will be overestimated.

Wofsy et al.'s[11] partition coefficient of 0.3 is much too large. Because these authors did not control their crystal growth conditions, they probably produced constitutional supercooling, resulting in an overestimation of K. Another possibility is that, as observed by Oguro and Igashi,[64] the propagation of the steps responsible for crystal growth[65] can be stopped because of solute concentration at the edge of the step. The next growth step can then catch up to the underlying inhibited step, thus trapping excess amounts of solute. Unlike the case when dendrites form following the breakdown of the growth interface, such growth and trapping pattern need not result in a suspicious-looking "milky" crystal. The measured partition coefficient will nevertheless be much greater than the true value.

The study of Wolff et al.[47] reports a saturation solubility of less than 1.8×10^{-4} mole fraction at -74.7 °C (which was the detection limit of their energy-dispersive X-ray microanalyzer). Even though this result is only an upper limit, it is consistent with our results.

Our partition coefficient is in fact lower than found in previous studies (about 10^{-4} between 273 and 200 K) and also shows nonmonotonous variations with temperature, which we must try to explain. Clearly, because the parameter n is different in the liquid (n_l) and in the solid (n_s), K must be temperature dependent. More quantitatively, the data of Figure 8 can be explained by considering eq 10, details of which can be found in Wofsy et al.[11] and references therein.

$$n_1 \frac{\mathrm{d} \ln K}{\mathrm{d}(1/T)} = \frac{\Delta h^{s}_{HCl} - \Delta h^{v}_{HCl}}{R} + (n_1 - n_s) \frac{\mathrm{d} \ln S(T)}{\mathrm{d}(1/T)} \quad (10)$$

Again $S(T)$ is the solidus composition. Figure 8 shows that K rapidly increases as the temperature tends to 0 °C. At temperature close to 273.15 K, HCl is incorporated at infinite dilution in the liquid: the partial molar enthalpy of evaporation Δh^{v}_{HCl} is constant (74 kJ/mol) and $n_1 = 2$ (calculated from ref 50). Since $\Delta h^{s}_{HCl} = 63.7$ kJ/mol and $n_s = 2.73$, we have therefore $\mathrm{d} \ln K/\mathrm{d}(1/T) < 0$. At lower temperatures (270−230 K, i.e., the liquidus is between 10^{-2} and 10^{-1} mole fraction), calculations from ref 50 show that n_1 increases ($n_1 > 2.73$) and Δh^{v}_{HCl} decreases ($\Delta^{v}_{HCl} < 64$ kJ/mol at 230 K) and we therefore have $\mathrm{d} \ln K/\mathrm{d}(1/T) > 0$ (relation 10). $\mathrm{d} \ln K/\mathrm{d}(1/T) = 0$ occurs at temperatures close to 270 K where n has roughly the same value in the liquid and in the solid (2.73). Relation 10 clearly shows that the temperature dependence of the partition coefficient is related to the number of defects ($n_l - n_s$) generated during the incorporation of HCl in the ice lattice and to Δh^{v}_{HCl}, which varies with T. Parameters in the solid do not vary, as deduced from our study of the gas to solid partitioning. On the contrary, parameters in the liquid vary and the change of trend in the variation of K with T shown in Figure 8 thus reflects the changing interactions between HCl and liquid H_2O as T and the liquid solution composition vary simultaneously along the phase boundary of Figure 7.

Incorporation Mechanism. Seidensticker[45] has related the concentration dependence of the partition coefficient to defects generated by a substitutional incorporation of HCl in the ice lattice. As observed in water, HCl may behave in ice like a strong electrolyte and be fully ionized. Some infrared spectroscopic data regarding the incorporation of HCl on the ice surface tend to support this hypothesis,[66,67] although it is not clear that those data apply to bulk ice at $T > 200$ K. Low-frequency conductivity measurements from Young[68] reported by Seidensticker[45] suggest also that HCl is dissociated. With the hypothesis that HCl substitutes for H_2O in the ice lattice, one implication is that HCl will introduce a Bjerrum L defect in the lattice (i.e., the absence of an H atom between two O atoms). The partition coefficient expected in this case is roughly consistent with Seidensticker's measurements. Therefore, as a result of its complete ionization and its substitutional incorporation, the HCl partial pressure over the solid solution is expected to be proportional to the cube of its concentration in the condensed phase and $n = 3$ in eq 3. However, this hypothesis is not supported by our value for n. HCl is then probably in interstitial sites as proposed for HF to account for its rapid diffusion in ice[69] or only partially dissociated if it is substitutional. An interstitial position may introduce lattice distortions. These may change the nature and concentration of point defects in the ice lattice but this point is difficult to confirm.[70] Structural information obtained by X-ray absorption fine structure spectroscopy would be helpful.

Solubility in the Solid Solution Domain. As indicated in Figure 7, solubilities predicted by our experiments are much lower than reported in most previous studies. As mentionned in the Introduction, the high values of Molina et al.[49] were due to the high P_{HCl} used, which resulted in the formation of a metastable HCl liquid solution. Likewise, the high values of Wofsy et al.[11] were based on an incorrect partition coefficient.

In a preliminary paper, Hanson and Mauersberger[48] have directly studied HCl partial pressure versus ice composition. However, they used Wofsy et al.'s partition coefficient[11] to constrain the fit of their data and obtained a solubility of 3×10^{-4} mole fraction under stratospheric conditions (200 K and 1.3×10^{-5} Pa). Moreover, the authors assume that at 200 K, their 1 μm thick ice film equilibrates by diffusion of HCl from the gas phase in less than 1 s. Our diffusion coefficient for HCl in ice at higher temperature (10^{-12} cm^2/s at -15 °C) suggests that their substrate may not have reached volume equilibrium. Using different substrate masses, Hanson and Mauersberger[51] have confirmed in a subsequent paper that they could not distinguish surface effects from volume solubilities in this preliminary work. They proposed another method to determine the solubility of HCl in ice under stratospheric conditions.

First, they have estimated the temperature dependence of P_{HCl} on the ice hexahydrate coexistence curve and found that at 190 K, $P_{HCl} = 3 \times 10^{-4}$ Pa. Second, they assumed that at 190 K, ice in equilibrium with the HCl hexahydrate has roughly the same composition as ice at the ice hexahydrate eutectic, i.e., $S = 3.5 \times 10^{-4}$ mole fraction (using the eutectic composition 0.1285 in mole fraction, Figure 1, and Gross et al.'s partition coefficient[46] $K = 0.0027$). Assuming that at a given temperature P_{HCl} is proportional to $(X_{HCl})^2$ ($n_s = 2$) in the solid solution, they find a solubility of 9×10^{-5} mole fraction at 190 K under $P_{HCl} = 2 \times 10^{-5}$ Pa. Under the same conditions, our data yield $X_{HCl} = 3 \times 10^{-5}$ mole fraction (eq 6) which is in reasonable agreement when we note that Hanson and Mauersberger's value must be considered as an upper limit, because (i) ice composition at the eutectic is probably lower because we find $K = 6 \times 10^{-4}$

at the eutectic point rather than $K = 0.0027$, ref 46); (ii) the solvus composition probably decreases at temperatures under the eutectic halt as observed in most phase diagrams that display a solid state miscibility gap[71] (this decrease is what Figure 7 suggests, as the isosolubility lines and the ice hexahydrate boundaries are in fact not quite parrallel); (iii) our data support a higher value for n_s which will also decrease the solubility predicted from ref 51.

Implications for the Air−Snow Transfer Function. Our thermodynamic results can be applied to the polar troposphere in order to study the HCl air−snow transfer function. HCl partial pressure in the summer Summit boundary layer (Central Greenland) have been measured using annular denuders[16,18,72] and mist chamber sampling technique.[19,73] Typical HCl partial pressure is around 2×10^{-6} Pa with reasonable agreement between those two different methods. Fresh snow samples have also been collected on the field and analyzed by ion chromatography. The HCl content in fresh deposited snow is typically 5×10^{-9} mole fraction. As the average summer air temperature at Summit is −15 °C, equilibrium solubility is expected to be 2.7×10^{-7} mole fraction (relation 6). Thus, the results presented here show that Greenland snow is undersaturated in HCl by a factor of about 40 and determining atmospheric composition from chloride content of snow cannot be achieved assuming equilibrium with the atmosphere.

Other incorporation processes occurring during the atmospheric phase of snowflakes have been proposed to explain snow composition.[15,18] Dominé et al.[18] have proposed that the HCl mole fraction in Greenland snow could be explained by condensation kinetics, i.e., by considering the number of HCl and H_2O molecules that hit and stick to the ice surface. X_{HCl} is then predicted to be

$$X_{HCl} = \frac{P_{HCl}}{P_{H_2O}} \frac{\alpha_{HCl}}{\alpha_{H_2O}} \left[\frac{M_{H_2O}}{M_{HCl}}\right]^{1/2} \qquad (11)$$

where α is the mass accomodation coefficient. Using $\alpha_{HCl} = 0.2$ for HCl, $\alpha_{H_2O} = 0.5$ for H_2O, and $P_{HCl}/P_{H_2O} = 2.2 \times 10^{-8}$ (ref 18), relation 13 gives $X_{HCl} = 6.2 \times 10^{-9}$ mole fraction, in reasonable agreement with the measured value of 5×10^{-9}. Other processes like no incorporation of HCl in vapor-grown ice and all of the HCl contained in a small fraction of the ice formed by riming of supercooled droplets may also explain the HCl content in fresh snow.[18] Since HCl diffusion coefficient is low at −15 °C (10^{-12} cm^2/s), solid state diffusion is too slow to allow equilibration which explains why collected crystals remain undersaturated.[18]

Implication for the Partitioning of HCl in Ice Clouds. Our results can also be applied to determine the partitioning of HCl in ice clouds such as type II PSCs, cirrus clouds and condensation trails of planes. Polar stratospheric clouds form during the winter in the polar stratosphere where typical temperature and HCl partial pressure are around $T = 190$ K and $P_{HCl} = 1.3 \times 10^{-5}$ Pa. Under those conditions, the bulk solubility predicted by our data is 2.6×10^{-5} mole fraction (relation 6). However, since Greenland summer snow formed around −15 °C is not in equilibrium with the atmosphere, and because the rate of solid state diffusion decreases with T (ref 15), the composition of ice PSCs is expected to be also determined by condensation kinetics. Using mass accomodation coefficients of 0.3 and 0.6 for HCl (ref 74) and H_2O (ref 75) at 190 K, and $P_{HCl}/P_{H_2O} = 2.5 \times 10^{-4}$ for the polar stratosphere, relation 11 gives $X_{HCl} = 8.8 \times 10^{-5}$ mole fraction which is higher than thermodynamic prediction by a factor of about 3.

HCl can also be located on the surface of ice particles. However, assuming a monolayer coverage of HCl on ice[74] and the ice surface area value in an ice PSC given by Turco et al.,[8] it appears that the fraction of HCl located on the ice surface is negligible.[76] It is interesting to predict the partitioning of HCl between the gas and ice phases depending on whether HCl incorporation is ruled by equilibrium or by condensation kinetics. For ice PSCs we have a volume fraction of ice particles of 10^{-10} m^3 of ice/m^3 of air.[8,12] The resulting partitioning of HCl is shown in Table 6. With typical lifetime and size of type II PSC's particle,[12] the small fraction of incorporated HCl will not diffuse through ice particles and can be considered as trapped regardless of which mechanism governs the formation of stratospheric ice crystals. If incorporation is ruled by kinetics, the depletion of gas phase HCl by the formation of type II PSC's particle[12] will be about 8.5%. Sedimentation of type II PSCs will then not lead to important dechlorination of the stratosphere and HCl will remain available for adsorption and heterogeneous reactions on ice surfaces.

TABLE 6: Partitioning (%) of HCl in Type II PSCs, Cirrus, and Condensation Trails of Planes

	fraction of HCl	equilibrium	kinetics
type II PSC	in the gas phase	97.2	91.5
	in the ice volume	2.8	8.5
cirrus	in the gas phase	65	88
	in the ice volume	35	12
contrail	in the gas phase	1.2	5.5
	in the ice volume	98.8	94.5

In the troposphere, cirrus clouds and high-altitude convective clouds[1] are also made up of ice crystals. Because of the expected increase in air traffic, aircraft condensation trails[2] have also recently received attention because they could enhance the appearance of high-altitude clouds. Typical temperature and HCl partial pressure conditions in cirrus are $T = 235$ K (ref 2) and $P_{HCl} = 3 \times 10^{-6}$ Pa (ref 77). Under those conditions, the equilibrium solubility is 9×10^{-7} mole fraction (eq 6), while condensation kinetics will incorporate 6.5×10^{-8} mole fraction (relation 11 using $\alpha_{HCl} = 0.3$ and $\alpha_{H_2O} = 0.6$; ref 74). The partitioning of HCl in cirrus clouds whose ice water content is 50 mg/m^3 (5×10^{-8} m^3/m^3, ref 2) is reported in Table 6.

Condensation trails generally form at higher altitudes where temperature is about 220 K (ref 78) and have a greater particle concentration than cirrus clouds, leading typically to 10^{-6} particle to air volume ratio a few minutes after formation.[78] The solubility predicted by our data (relation 6) at $T = 220$ K and $P_{HCl} = 3 \times 10^{-6}$ Pa is about 2×10^{-6} mole fraction. Incorporation by condensation kinetics will result in a composition of 4.1×10^{-7} mole fraction (relation 11). As shown in Table 6, ice particles can trap large amounts of atmospheric HCl in cirrus and condensation trails. Moreover, a lot of the HCl could be located on the ice surface because contrail particles are small crystals (30 μm corresponding to a surface area 0.2 m^2/m^3 of air, ref 2). Assuming a surface coverage of ice of about 0.01 monolayer,[76] 94% of the HCl will be located on the surface of ice particles. Since those clouds can seriously deplete the gas phase in HCl and doubtless in other trace gases that interact with ice, they potentially have an important impact on atmospheric chemistry. Understanding ice cloud chemistry therefore requires the knowledge of incorporation of trace gases in ice.

Acknowledgment. This work was supported by the Commission of the European community (contracts EV5V-CT91-0022 and EV5V-CT93-0336), CNRS (PAMOY program), Région Rhône-Alpes (contract X 071280004), and Université Joseph Fourier of Grenoble. We thank O. Brissaud for his help with the crystal growth, V. Rommelaere for his help with the

fitting of the data, and M. Pourchet for sharing his laboratory space. We also thank an anonymous reviewer for helpful and detailed comments.

References and Notes

(1) Hobbs, P. V.; Rangno, A. L. *J. Atmos. Sci.* **1985**, *42*, 2523.

(2) Gayet, J.-F.; Febvre, G; Brogniez, G.; Chepfer, H.; Renger, W.; Wendling, P. *J. Atmos. Sci.* **1996**, *53*, 126.

(3) Solomon, S.; Garcia R. R.; Rowland, F. S.; Wuebbles, D. J. *Nature* **1986**, *321*, 755.

(4) Molina, M. J. *Atmos. Environ., Part A*, **1991**, *25*, 2535.

(5) Molina, M. J. In *The Chemistry of the Atmosphere: Its impact on Global Change*; Calvert, J. G., Ed.; Blackwell Scientific: Boston, MA, 1994; p 27.

(6) Fahey, D. W.; Kelly, K. K.; Ferry, G. V.; Poole, L. R.; Wilson, J. C.; Murphy, D. M.; Loewenstein, M. Chan, K. R. *J. Geophys. Res.* **1989**, *94*, 11229.

(7) Hanson, M.; Mauersberger, K. *J. Phys. Chem.* **1988**, *92*, 6167.

(8) Turco, R. P.; Toon, O. B.; Hamill, P. *J. Geophys. Res.* **1989**, *94*, 16493.

(9) MacKenzie, A. R.; Kulmala, M.; Laaksonen, A.; Vesala, T. *J. Geophys. Res.* **1995**, *100*, 11275.

(10) Toon, O. B.; Hamill, P.; Turco, R. F.; Pinto, J. *Geophys. Res. Lett.* **1986**, *13*, 1284.

(11) Wofsy, S. C.; Molina, M. J.; Salawitch, R. J.; Fox, L. E.; McElroy, M. B. *J. Geophys. Res.* **1988**, *93*, 2442.

(12) Goodman, J.; Toon, O. B.; Pueschel, R. F.; Snetsinger, K. G.; Verma, S. *J. Geophys. Res.* **1989**, *94*, 16449.

(13) Solomon, S. *Rev. Geophys.* **1988**, *26*, 131.

(14) (a) Solomon, S. *Nature* **1990**, *247*, 357. (b) Nickolaisen, S. L.; Friedl, R. R.; Sander, S. P. *J. Phys. Chem.* **1994**, *98*, 155.

(15) (a) Dominé, F.; Thibert, E.; Van Landeghem, F.; Silvente, E.; Wagnon, P. *Geophys. Res. Lett.* **1994**, *21*, 601. (b) Dominé, F.; Thibert, E. *Geophys. Res. Lett.* **1996**, *24*, 3627.

(16) Legrand, M. In *Low-Temperature Chemistry of the Atmosphere*; Moortgat, G., *et al.* Ed.; NATO ASI: Series I, 1994; Vol. 21, p 421.

(17) Sigg, A.; Staffelbach, T.;, A. *J. Atmos. Chem.* **1992**, *14*, 223.

(18) Dominé, F.; Thibert, E.; Silvente, E.; Legrand, M.; Jaffrezo, J.-L. *J. Atmos. Chem.* **1995**, *21*, 165.

(19) Legrand, M.; Leopold, A.; Dominé, F. In *Processes of chemical exchange between the atmosphere and polar snow*; Wolff, E., Bales, R. C. Eds.; Springer: Berlin, 1996; NATO ASI Series I, Vol. 43, p 19.

(20) Buat-Ménard, P.; Morelli, J.; Chesselet, R. *J. Res. Atmos.* **1974**, *8*, 661.

(21) Fitzgerald, J. W. *Atmos. Environ.* **1991**, *25A*, 533.

(22) Fenter, F. F.; Caloz, F.; Rossi, M. *J. Phys. Chem.* **1994**, *98*, 9801.

(23) Legrand, M.; Delmas, R. *J. Geophys. Res.* **1988**, *93*, 7153.

(24) Legrand, M.; Delmas, R. *Atmos. Environ.* **1984**, *18*, 1867.

(25) De Angelis, M.; Legrand, M. In *Ice core chemistry of global biogeochemistry cycles* Delmas, R. J., Ed.; Springer-Verlag: Berlin, 1994; NATO ASI Series I, Vol. 30, p 369.

(26) Johannessen, M.; Dale, T.; Gjessing, E. T.; Henriksen, A.; Wright, R. F. *Proceedings of Isotopes and Impurities in Snow and Ice*, Grenoble; International Association of Sci. Hydrology Publication; 1975; Vol. *118*, p 116.

(27) Johannessen, M.; Henriksen, A. *Water Resources Res.* **1978**, *14*, 615.

(28) Tranter, M. P.; Brimblecombe, P.; Davies, T. D.; Vincent, C. E.; Abrahams, P. W.; Blackwood I. *Atmos. Environ.* **1986**, *20*, 517.

(29) Brimblecombe, P.; Clegg, S. L.; Davies, T. D.; Shooter, D.; Tranter, M. *Water Resources* **1988**, *22*, 693.

(30) Hewitt, A. D.; Cragin J. H.; Colbeck S. C. *Proc. Forty-Six Annu. Eastern Snow Conf., Quebec City, Quebec*, **1989**. 165.

(31) Cragin, J. H.; Hewitt A. D.; Colbeck S. C. *CRREL Rep.* **1993**, *93*−8, 20.

(32) Dominé, F.; Thibert, E. In *Biogeochemistry of seasonally snow-covered catchments*; IAHS Publ. No. 228; Tonnesen,K., Williams, M., Tranter, M., Eds.; IAHS Press: Wallingford, U.K., 1995; p 3.

(33) Pickering, S. U. *Ber. Dtsch. Chem. Ges.* **1893**, *26*, 277.

(34) Rupert, F. *J. Am. Chem. Soc.* **1909**, *31*, 851.

(35) Vuillard, G. *C. R. Acad. Sci.* **1955**, *241*, 1308.

(36) Ji, K. Etude de la composition des aérosols stratosphériques polaires au moyen des diagrammes de phase stables, métastables et cinétiques des systèmes: HNO_3/H_2O, HCl/H_2O et H_2SO_4/H_2O. Thesis, Université de Paris VII, Paris, 1994.

(37) Lliboutry, L. *Traité de Glaciologie*; Masson & Cie éditeurs: Paris, 1964; Vol. 1, Chapter I.

(38) Workman, E. J.; Reynolds, S. E. *Phys. Rev.* **1950**, *78*, 254. Zaromb, S.; Brill, R. *J. Chem. Phys.* **1956**, *24*, 895.

(39) Jaccard, C.; Levi, L. *Z. Angew. Math. Phys.* **1961**, *12*, 70. Brill, R. *SIPRE Rep.* **1957**, *33*, 67.

(40) Gränicher, H. *Helv. Phys. Acta* **1963**, *28*, 300.

(41) Gross, G. W. *J. Colloid Interface Sci.* **1967**, *25*, 270.

(42) Dorlot, J. M.; Baïlon, J. P.; Masounave, J. *Des matériaux*; Editions de l'Ecole Polytechnique de Montréal: Quebec, 1986; Chapter V.

(43) Krishnan, P. N.; Salomon, R. E. *J. Phys. Chem.* **1969**, *73*, 2680.

(44) De Micheli, S. M.; Iribarne, J. V. *J. Chim. Phys.* **1963**, *60*, 767.

(45) Seidensticker, R. G. *J. Chem. Phys.* **1972**, *56*, 2853.

(46) Gross, G. W.; Wong, P. W.; Humes, K. *J. Chem. Phys.* **1977**, *67*, 5264.

(47) Wolff, E. W.; Mulvaney, R.; Oates, K. *Geophys. Res. Lett.* **1989**, *16*, 487.

(48) Hanson, M.; Mauersberger, K. *Geophys. Res. Lett.* **1988**, *15*, 1507.

(49) (a) Molina, M. J.; Tso, T. L.; Molina, L. T.; Wang, F. C. Y. *Science* **1987**, *238*, 1253. (b) Abbatt, J. P. D.; Beyer, K. D.; Fucaloro, A. F.; McMahon, J. R.; Wooldridge, P. J.; Zhang, R.; Molina, M. J. *J. Geophys. Res.* **1992**, *97*, 15819.

(50) Fritz, J. J.; Fuget, C. R. *Ind. Eng. Chem., Chem. Eng. Data Ser.* **1956**, *1*, 10.

(51) Hanson, M.; Mauersberger, K. *J. Phys. Chem.* **1990**, *94*, 4700.

(52) Hobbs, P. V. *Ice Physics*; Clarendon Press: Oxford, U.K., 1974; Chapter IX.

(53) Legrand, M.; De Angelis, M.; and Maupetit, F. *J. Chromatogr.* **1993**, *640*, 251.

(54) (a) Hobbs, P. V. *Ice Physics*; Clarendon Press: Oxford, U.K., 1974; Chapter IV. (b) Duval, P.; Ashby, M. F.; Anderman, I. *J. Phys. Chem.* **1983**, *87*, 4066. (c) Ahmad, S.; Whitworth, R. W. *Phil. Mag.* **1988**, *57*, 749.

(55) Philibert, J. *Diffusion et transport de matière dans les solides*; Les éditions de physique: Les Ulis, France, 1990; Chapter I.

(56) Badrour, L.; Moya, E. G.; Bernardini, J.; Moya, F. *J. Phys. Chem. Solids* **1989**, *50*, 551.

(57) Hobbs, P. V. *Ice Physics*; Clarendon Press: Oxford, U.K., 1974; Chapter II.

(58) Weast, R. C., Ed. *CRC Handbook*; CRC Press: Boca Raton, FL, 1973.

(59) Walrafen, G. E.; Yang, W.-H.; Chu, Y. C.; Hokmabadi, M. S.; Carlon, H. R. *J. Phys. Chem.* **1994**, *98*, 4169.

(60) Wooldridge, P. J.; Zhang, R.; Molina, M. J. *J. Geophys. Res.* **1995**, *100*, 1389.

(61) Koehler, B. G.; Middlebrook, A. M.; Tolbert M. A. *J. Geophys. Res.* **1992**, *97*, 8065.

(62) Christian, J. W. *The theory of transformations in metals and alloys*; Pergamon Press: Oxford, U.K., 1965; Chapter XIV.

(63) Tiller, W. A.; Jackson, K. A.; Rutter, J. W.; Chalmers, B. *Acta Met.* **1953**, *1*, 428.

(64) Oguro, M.; Igashi, A. *Philos. Mag.* **1971**, *24*, 713.

(65) Ketcham, W. M.; Hobbs, P. V. *Philos. Mag.* **1968**, *18*, 659.

(66) Horn, A. B.; Chester, M. A.; McCoustra, M. R. S.; Sodeau, J. R. *J. Chem. Soc., Faraday Trans.* **1992**, *88*, 1077.

(67) Delzeit, L. A.; Rowland, B.; Devlin, J. P. *J. Phys. Chem.* **1993**, *97*, 10312.

(68) Young, I. G. Ph.D. Thesis, Temple University, Philadelphia, PA, 1968.

(69) Kopp, M.; Barnaal, D. E.; Lowe, I. J. *J. Chem. Phys.* **1965**, *43*, 2965.

(70) Gross, G. W.; Gutjahr, A.; Caylor, K. *J. Phys. Colloid* **1987**, *C1*, 527.

(71) Lupis, C. H. P. *Chemical Thermodynamics of Materials*, Elsevier Science Publishing Co., Inc.: New York, 1983; Chapter VIII.

(72) Silvente, E. *Contribution à l'étude de la fonction de transfert air-neige en régions polaires*; Thesis, Université Joseph Fourier, Grenoble, France, 1993.

(73) Leopold, A. *Contribution à l'étude de la fonction de transfert air-neige pour les gaz acides (acides organiques, HNO_3, HCl)*; Thesis, Université Joseph Fourier, Grenoble, France, 1995.

(74) Hanson, D. R.; Ravishankara, A. R. *J. Phys. Chem.* **1992**, *96*, 2682.

(75) Haynes, D. R.; Tro, N. J.; George, S. M. *J. Phys. Chem.* **1992**, *96*, 8502.

(76) Dominé, F.; Chaix, L.; Thibert, E. Air pollution research report 56, Polar stratospheric ozone. *Proceedings of the 3rd European Workshop, September 1995, Schliersee, Germany*; Published by the European community, 1996; p 736.

(77) Vierkorn-Rudolph, B.; Bächmann, K.; Schwartz, B.; Meixner, F. X. *J. Atmos. Chem.* **1984**, *2*, 47.

(78) Danilin, M. Y.; Ebel, A.; Elbern, H.; Petry, H. *J. Geophys. Res.* **1994**, *99*, 18951.